PAPER

Check for updates

A novel strategy for the characterization of glaucocalyxin A metabolites *in vivo* and *in vitro* by UHPLC-Q-TOF-MS based on DDA and DIA data acquisitions

Wenjing Sun,[a] Yiran Jin,[b] Shuai Guan,[b] Mengxin Yang,[a] Miaoting Zhang,[a] Jiali Hou[a] and Yingfeng Du [ID] *[a]

Glaucocalyxin A (GLA) belongs to the natural ent-kauranoid diterpenoids family with antitumor, antifibrotic, anticoagulative, antioxidant, and anti-AD effects. In this study, ultra-high-performance liquid chromatography coupled to quadrupole time-of-flight mass spectrometry (UHPLC-Q-TOF-MS) system was applied to observe probable metabolites of GLA *in vitro* and *in vivo* firstly. The mass data were respectively obtained by two typical acquisition methods, 'data-dependent acquisition' (DDA) and 'data-independent acquisition' (DIA) modes. The combinations can not only guarantee sensitivity but also capture more precursor ions and MS/MS spectra. Then, multiple data processing techniques were applied to hunt metabolites rapidly. As a result, 32 phase I metabolites of different structures and 6 phase II metabolites were identified, including 25, 18, 17 and 7 in rat urine, feces, bile, and plasma, respectively. Besides, under the action of rat intestinal flora (RIF), 7 metabolites were detected. In the study, the main bio-transformations were oxidation and demethylation. Conjugation with methylation, sulfate, and glucuronide produced phase II metabolites. This study laid the foundation for the further study of the pharmacological effects of GLA and was conducive to mechanism research.

1. Introduction

Rabdosia japonica has been extensively used as an oriental medicine and dietary supplement in Asia.[1] For thousands of years, it has been used for the treatment of gastrointestinal floral infections.[2–4] Glaucocalyxin A (GLA), an ent-kauranoid diterpenoid, derives from the *Rabdosia japonica* plant. Diterpenoids, triterpenoids, and flavonoids are the main components of the herb.[5] Moreover, GLA is the most active diterpenoid, acting as a quality index of this herb.[2] Nowadays, GLA has aroused widespread concern by scientists in various fields due to its multiple antitumor,[6–10] antifibrotic,[11] anticoagulative,[12] antioxidant,[13] and anti-AD effects.[14]

The absorbance and elimination of GLA in rats were fast after oral administration ($T_{max} = 0.750 \pm 0.224$ h, $t_{1/2} = 1.11 \pm 0.17$ h).[2] The excretion of GLA amounted to 23.8%, 12.8% and 35.68% in feces, urine, and bile within 12 h respectively.[15] These results indicated that GLA was fast metabolized and excreted mainly as metabolites. To our knowledge, only eight metabolites and three metabolite transformation types of GLA

[a]Department of Pharmaceutical Analysis, School of Pharmacy, Hebei Medical University, 361 East Zhongshan Road, Shijiazhuang, Hebei 050017, P. R. China. E-mail: yingfengdu@126.com; Fax: +86-311-86266419; Tel: +86-311-86265625
[b]The Second Hospital of Hebei Medical University, Shijiazhuang, Hebei 050000, P. R. China

were identified in rat bile and rat liver microsome by HPLC-MS-ESI. And there was few systematic summary of metabolic profiles.[16]

Some transformations of Traditional Chinese Medicine (TCM) orally administered were under the action of intestinal flora in the gastrointestinal tract. Accordingly, in exoteric metabolite research, intestinal flora has been extensively used.[17,18] Besides, scientists usually predict the metabolic profile in humans by microbial transformation.[19]

Although ultra-high-performance liquid chromatography coupled to quadrupole time of flight mass spectrometry (UHPLC-Q-TOF-MS) has played an essential role in qualitative studies with higher sensitivity and accuracy, excavation trace metabolites in complex biological matrices were still facing huge challenges. Feature fragments provided by the mass spectrometer is vital for judging metabolite elemental composition and inferring structure. Generally speaking, the hit rate and quality of the MS/MS spectrum are the key information for identifying metabolites. The MS information was obtained by full scan, while available MS/MS spectrum acquisition techniques in LC/MS can roughly be divided into two categories: data-dependent acquisition (DDA) and data-independent acquisition (DIA). In order to obtain the MS/MS spectrum of as many metabolites as possible, we innovatively combined the two methods in this experiment.

The DDA method is also called the IDA method in some literature. When using the DDA method, the criteria and the mass defect filtering (MDF) filter templates must be pre-set. The occurrence of the MS/MS spectrum is dependent on the preset criteria to a great extent. Despite its ability to obtain a high-quality MS/MS spectrum, there are many defects such as exploring the template setup method, understanding the metabolic transformation theory, and setting a reasonable level. A high-quality MS/MS spectrum of a target compound cannot be obtained unless its amount exceeds the preset criteria. Given the above reasons, the hit rates of the MS/MS spectrum in the DDA method are lower but the quality is high.

SWATH (sequential window acquisition of all theoretical fragment ion spectra) is a commonly used DIA technique in AB Sciex. The DIA method does not need to set thresholds in advance. All signals enter the collision chamber in turn to obtain the MS/MS spectrum. Therefore, it can sequentially acquire the MS/MS spectrum of whole precursor ions, which greatly increases the hit rate of the MS/MS spectrum of trace substances. However, it is a disadvantage that the missing preselection may result in impure mass spectra, which may be difficult to identify and lead to a decreasing sensitivity.[20] Therefore, the combination of the above two methods will increase not only the quality of the MS/MS spectrum but also the hit rate of trace metabolites. Therefore, it could increase the number of metabolites identified and enrich metabolic profile.

In this study, a practical method combined with DDA and DIA acquisitions was established and developed to identify metabolites of GLA *in vivo* and *in vitro* by UHPLC-Q-TOF-MS for the first time. Besides, we compared these two data acquisitions to demonstrate the advantages. Finally, the rapid UPLC-Q-TOF-MS based on multiple data processing technologies was successfully employed to expound metabolites and metabolic profile of GLA.

2. Experiments

2.1 Reagents and materials

GLA (purity ≥ 98%) was purchased from Weikeqi Chemical Industry (Sichuan, China). HPLC-grade formic acid and acetonitrile were both purchased from Fisher (NJ, USA), and ultra-pure water was purchased from Wahaha Corporation (Hangzhou, China). L-Cysteine, L-ascorbic acid, CMC-Na, $MgCl_2$, K_2HPO_4, KH_2PO_4, NaCl, $(NH_4)_2SO_4$, $CaCl_2$, $MgSO_4$, and Na_2CO_3 were from Beijing AoBoXing Biotech Co., Ltd. (Beijing, China).

2.2 Instrumentation and analytical conditions

Chromatographic separation was performed on a Shimadzu (Kyoto, Japan) UPLC instrument including a binary solvent delivery system (LC-30AD), an auto sampler (SIL-30AC), and a column oven (CTO-30A). The chromatographic system was performed on a Phenomenex Luna C18 (2.6 μm, 100 mm × 3.0 mm) attached to a guard column and the column temperature was maintained at 25 °C. The mobile phase consisted of water (A) and acetonitrile (B). Both solutions were supplemented with 0.1% formic acid. Linear gradient elution was set as the

procedure: 0–20 min, 18–38% B; 20–23 min, 38–45% B; 23–28 min, 45–65% B; 28–31 min, 65–90% B, 31–35 min, 90% B. The initial proportional concentration maintained for 10 minutes before the next sample was collected. The injection volume was 3 μL and the flow rate was 0.4 mL min^{-1}.

Besides, mass spectrometry was executed on a Triple TOF™ 5600+ system with Duo-Spray™ ion sources operating in the negative electrospray ionization (ESI) mode. Analyst® TF 1.7 software was used to control the instrument and for data acquisition.

The specific parameters of MS and MS/MS were listed in Table 1, and these two modes have similarities and differences.[21] All samples were detected with electrospray ionization (ESI) source in negative ionization mode. Besides, a superb calibration delivery system (CDS) was used to automatically check the MS and MS/MS during the acquisition time.

2.3 Metabolism of GLA by rat intestinal flora (RIF) *in vitro*[22,23]

2.3.1 Solution preparation. GLA was dissolved in the methanol solution to obtain 1 mg mL^{-1} GLA solution.

2.3.2 Preparation of anaerobic medium. Solution A (19 mL, 0.78% K_2HPO_4, 0.48% KH_2PO_4, 1.18% NaCl, 1.20% $(NH_4)_2SO_4$, 0.12% $CaCl_2$, 0.25% $MgSO_4 \cdot H_2O$), solution B (25 mL, 8% Na_2CO_3). L-Cysteine (0.25 g), L-ascorbic acid (0.25 g), eurythrol (0.5 g), tryptone (0.5 g) and nutrient agar (0.5 g) were mixed and diluted with ultra-pure water to 500 mL. Adjust the pH with hydrochloric acid to 7.5–8.0 before autoclaving.

2.3.3 Preparation of intestinal flora culture medium. Firstly, 1 g fresh rat feces was taken and 10 mL anaerobic medium was added to a tube. After stirring uniformly, it was filtered with gauze to obtain a supernatant, that is, intestinal flora culture medium.

2.3.4 Metabolism of GLA *in vitro*. The culture medium (1 mL) and 1 mg mL^{-1} GLA (100 μL) were added to the centrifuge tube filled with N_2. Then incubated at 37 °C for 24 h. After that, 3 mL of acetic ether was added and vortexed for 2 min. The samples were centrifuged at 15 000 rpm for 10 min. Nitrogen was used to evaporate the supernatant. The residue was dissolved in 200 μL mobile phase and filtered with the organic membrane of 0.22 μm. Finally, the filtrate was transferred to a sample vial to run an analysis.

At the same time, there were two control groups: blank B (100 μL methanol in culture medium fluid) and blank C (100 μL GLA in anaerobic medium fluid), see Fig. 3.

2.4 Metabolism of GLA *in vivo*

2.4.1 Bio-sample collection. Thirty-six male Sprague Dawley (SD) rats (Certificate No. 11400700340317, 12–13 weeks), weighing 230 ± 20 g, were purchased from Beijing Vital River Laboratory Animal Technology Co. Ltd (Beijing, China). The experiment strictly complied with the Animal Ethics Committee at the Institute of Hebei Medical University. The procedures were under the Guide for the Care and Use of Laboratory Animals of the National Institutes of Health. All rats have free access to standard water and food in a standardized animal

Table 1 The parameters of MS and MS/MS analysis

		DDA (negative)	DIA (negative)
Different parameters	Accumulation time of MS (ms)	200	430
	Accumulation time of MS/MS (ms)	100	60
	The number of isolation windows	0	28
	The wide of isolation windows (Da)	0	26
	The cycle time (s)	1.0499	1.2973
	The cycles	1772	1434
Common parameters	Declustering potential (eV)	−60	−60
	Collision energy of MS/MS (eV)	−35	−35
	Collision energy spread (eV)	−15	−15
	Mass of TOF (Da)	100–800	100–800
	Mass of MS/MS (Da)	60–800	60–800
	Ion spray voltage floating (V)	−4500	−4500
	Nebulizing gas (psi)	55	55
	Heater gas (psi)	55	55
	Curtain gas (psi)	35	35
	Turbo spray temperature (°C)	550	550
	Mass acquisition time (min)	30	30

room. There were 8 days for them to accommodate the new environment.[24] After fasting for 12 hours, the rats were orally administered.

The rats were randomly divided into six groups with six rats in each group. Group 1, 3, and 5 were blank groups. Group 2, 4, and 6 were experimental groups. A single dose of GLA (suspended in 0.5% CMC-Na) was 10 mg kg^{-1}.[25] The rats of the blank groups were given 0.5% CMC-Na. Considering that many drugs are metabolized within 24 hours, our biological samples covered at least 24 h.[26]

Rats in groups 1 & 2 were held in metabolic cages to collect the urine and feces samples within 72 h. Rats in groups 3 & 4 were to collect bile under anesthesia within 24 h. The tubes used to collect urine, feces, and bile were placed in an ice bath, samples were collected as timely as possible. Rats in groups 5 & 6 were collected blood samples from the orbital vein of the rats with heparinized tubes at 0.25, 0.5, 0.75, 1, 2, 4, 8, 12 and 24 h after dosing.[2] Then all the blood samples were immediately centrifuged at 4500 rpm for 10 min under 4 °C to obtain plasma. The same biological sample was mixed and then stored at −80 °C.

2.4.2 Bio-sample preparation. For plasma and bile samples, two milliliters of plasma and 20 mL bile were respectively vortexed with 3-fold acetonitrile for 10 min to precipitate proteins. Before the supernatant was evaporated to dryness under N$_2$, it was centrifuged at 15 000 rpm for 10 min.

Six-fold (volume) ethyl acetate was added to lyophilized feces samples. The samples were vortexed, centrifuged, and took the supernatant, repeated 3 times. The supernatant was evaporated to dryness.

Besides, ten milliliters of urine and 3-fold ethyl acetate were vortexed for 10 min. Before the supernatant was evaporated to dryness under N$_2$, it was centrifuged at 15 000 rpm for 10 min.

The residue was dissolved in 200 μL mobile phase. Finally, the filtrate was transferred to a sample vial to run the analysis.

2.5 Analytical strategy and metabolite analysis[27–30]

The research strategy consisted of four steps: (1) on-line data were respectively acquired by both DDA and DIA mode. (2) These two sets of raw data were processed separately. Multiple post-data-processing technologies can eliminate hybrid spectra and detect metabolites rapidly.

As is known that DIA has high hit rates of the MS/MS spectrum compared to the DDA method. Combined with Principal Component Variable Grouping (PCVG) filtering in the MetabolitePilot™ post-processing software, the quality of the MS/MS spectrum could be greatly improved. KPIs technique, as an assistant tool in MasterView™1.1 software, could also detect metabolites with similar structures. In general, compounds that showed the same mother nucleus could exhibit similar fragmentation behaviors in collision induced dissociation mode due to their identical skeleton. Thus they can generate certain common fragments, namely key product ions (KPIs). The KPIs were preliminarily constructed by summarizing the mass fragmentation rules of the GLA. We set fragment ions at m/z 149.0594, 123.0450, 97.0670 as KPIs, because they were major and stable fragment ions. Given the most metabolites own the skeleton of their corresponding parent compounds, KPIs could be also used for the rapid detection and identification of the prototypes and their corresponding metabolites. With the assistant tool in MasterView™, we use KPIs as screening indicators. In this way, we can quickly target metabolites. Besides, other data mining methods including fragment ion filter (PIF), extract ion chromatogram (EIC), neutral loss filter (NLF), and mass defect filter (MDF) provided by the metabolic software were also applied. (3) Mass spectrometry is not suitable for isomer discrimination. The third step was the differentiation of isomers, we used two widely accepted parameters, namely, Clog P and the minimum capacity values. It is extremely troublesome to distinguish the structural isomers in the identification process of metabolites because of the same molecular formula, small difference in the retention time and the MS/MS

spectra. Therefore, a useful parameter Clog P calculated by the program Chemdraw Ultra 14.0 was introduced to distinguish the structural isomers. Usually, the compound with the less Clog P value had the shorter retention time in a reversed phase liquid chromatography system. We can make a preliminary distinction between isomers in this way. Besides, the minimum capacity values (software Chem3D) selected compound by calculating the values at different sites of the group. (4) Finally, relevant drug bio-transformation knowledge is necessary.

3. Results and discussion

3.1 Mass spectrometric patterns of GLA (M0)

The chemical structure of **M0** was shown in Fig. 1. **M0** was eluted at 13.41 min and exhibited $[M - H]^-$ at m/z 331.1918 (0.9 ppm, elemental composition $C_{20}H_{28}O_4$) in all experimental samples under the chromatographic and mass conditions.

The deprotonated ion at m/z 331.1918 ($[M - H]^-$) of **M0** successively eliminated H_2O and CO to produce characteristic products ions at m/z 313.1819 ($[M - H–H_2O]^-$) and 285.1857 ($[M - H–H_2O–CO]^-$), respectively. Besides, the fragment ion at m/z 269.1898 ($[M - H–H_2O–CO_2]^-$) originating from the ion m/z 313.1819 ($[M - H–H_2O]^-$) was interpreted as proceeding via the loss of the C7 hydroxyl and the C15 carbonyl groups to remove the neutral fragment CO_2. Furthermore, the characteristic daughter ion at m/z 149.0594 ($[C_9H_{10}O_2–H]^-$) was acquired from the fracture of the C_7–C_8 bond and C_9–C_{10} bond. Key product ions (KPIs) were at m/z 149.0594, 123.0450, and 97.0670. Besides, another fragment ion was at m/z 297.1504 ($[M - H–H_2O–O]^-$). The MS/MS spectrum of deprotonated GLA and its fragmentation pathway were shown in Fig. 2.

It is general that a site with a high density of electron clouds is easily oxidized and where the electron cloud density is small is easy to be restored. Moreover, the carbon–carbon double bonds of **M0** predicted that hydrogenation and internal hydrolysis would occur, –OH predicted that loss of water, methylation, sulfate conjugation and glucuronide conjugation would occur.

3.2 Phase I metabolites identification

Most of phase I metabolites underwent oxidation, demethylation, ketone formation, hydrogenation, and internal hydrolysis. Ketone formation, oxidation, and oxidation to carboxylic acid

Fig. 1 Chemical structure of GLA.

can be thought of as the characteristic metabolic profile of **M0**. Other metabolic profiles were also observed.

3.2.1 Mono-oxidation metabolites. **M15** (t_R = 3.01 min), **M16** (t_R = 4.02 min), and **M17** (t_R = 22.25 min) had the same deprotonated ion $[M - H]^-$ at m/z 347 ($C_{20}H_{28}O_5$). The deprotonated ion at m/z 347 ($[M - H]^-$) of **M15–M17** successively eliminated H_2O and CO to produce characteristic products ions at m/z 329 ($[M - H–H_2O]^-$) and 301 ($[M - H–H_2O–CO]^-$), respectively. Next, the product ion at m/z 285 ($[M - H–H_2O–CO_2]^-$) was formed by the loss of CO_2 from the ion at m/z 329. In **M15**, the KPIs at m/z 149 and 123 were the same as **M0**. These showed that the mono-oxidation was not connected to A ring or C ring. Therefore **M15** was concluded occurred in the B ring. Based on the stereo hindrance effect and the oxidation theory, the potential position were at C-6. In **M16**, fragment ion was detected at m/z 165, indicating that mono-oxidation occurred in the C ring. According to the oxidation reaction theory, the 13-position was easily oxidized. After the oxidation of the C ring produced the ion at m/z 165, dehydration of two adjacent hydroxyl groups produced the ion at m/z 147, which can further confirm that the oxidation reaction occurred at C-13. In **M17**, the fragment ion at m/z 139 indicated that mono-oxidation occurred in the A ring. Given that a methyl group is an electron-donating group and the carbonyl group is an electron-withdrawing group, a site having a larger electron cloud density is liable to undergo an oxidation reaction. Thus the oxidation reaction of **M17** probably occurred at C-1.

3.2.2 Di-oxidation metabolites. **M18** (t_R = 11.62 min) and **M19** (t_R = 13.25 min) showed the same deprotonated ion $[M - H]^-$ at m/z 363 ($C_{20}H_{28}O_6$). The molecular weight was 32 Da (2O) higher than that of **M0**. The deprotonated ion at m/z 363 ($[M - H]^-$) of **M18–M19** successively eliminated H_2O and CO to produce characteristic products ions at m/z 345 ($[M - H–H_2O]^-$) and 317 ($[M - H–H_2O–CO]^-$), respectively. Then, the product ion at m/z 301 ($[M - H–H_2O–CO_2]^-$) was formed by the loss of CO_2 from the ion at m/z 345. Besides, **M18** and **M19** both produced the fragment ion at m/z 165, indicating that oxidation occurred in the C ring and one of the other two rings. According to the results of mono-oxidation metabolites, C-1, C-13, and C-6, C-13 positions were more likely to undergo di-oxidation reaction. It is extremely troublesome to distinguish the structural isomers because their MS/MS spectra were very similar. With the help of Clog P, they were initially deduced. The Clog P values of **M18** and **M19** were 0.5558 and 1.1302, respectively.

3.2.3 Tri-oxidation metabolites. Metabolite **M20** ($C_{20}H_{28}O_7$) was eluted at 23.14 min, which exhibited deprotonated molecular ion $[M - H]^-$ at m/z 379. The identical molecular formula was by means of the data post-processing software MetabolitePilot™. The deprotonated ion at m/z 379 ($[M - H]^-$) of **M20** successively eliminated H_2O and CO to produce characteristic products ions at m/z 361 ($[M - H–H_2O]^-$) and 333 ($[M - H–H_2O–CO]^-$), respectively. Afterwards, the product ion at m/z 317 ($[M - H–H_2O–CO_2]^-$) was formed by the loss of CO_2 from the ion at m/z 361. Fragment ions at m/z 165 and 139 implied that the metabolites underwent mono-
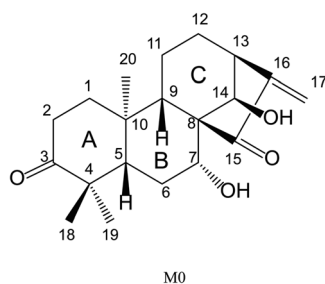
oxidation in the C ring and A ring, respectively. Referring to the likely sites of the mono-oxidation reaction, the position of tri-oxidation were at C-1, C-6, and C-13.

3.2.4 Ketone formation. M21, M22 and **M23** were eluted at 7.98 min, 8.23 min, and 8.44 min, respectively. Their identical molecular formula was $C_{20}H_{26}O_5$, 14 Da higher than **M0** by
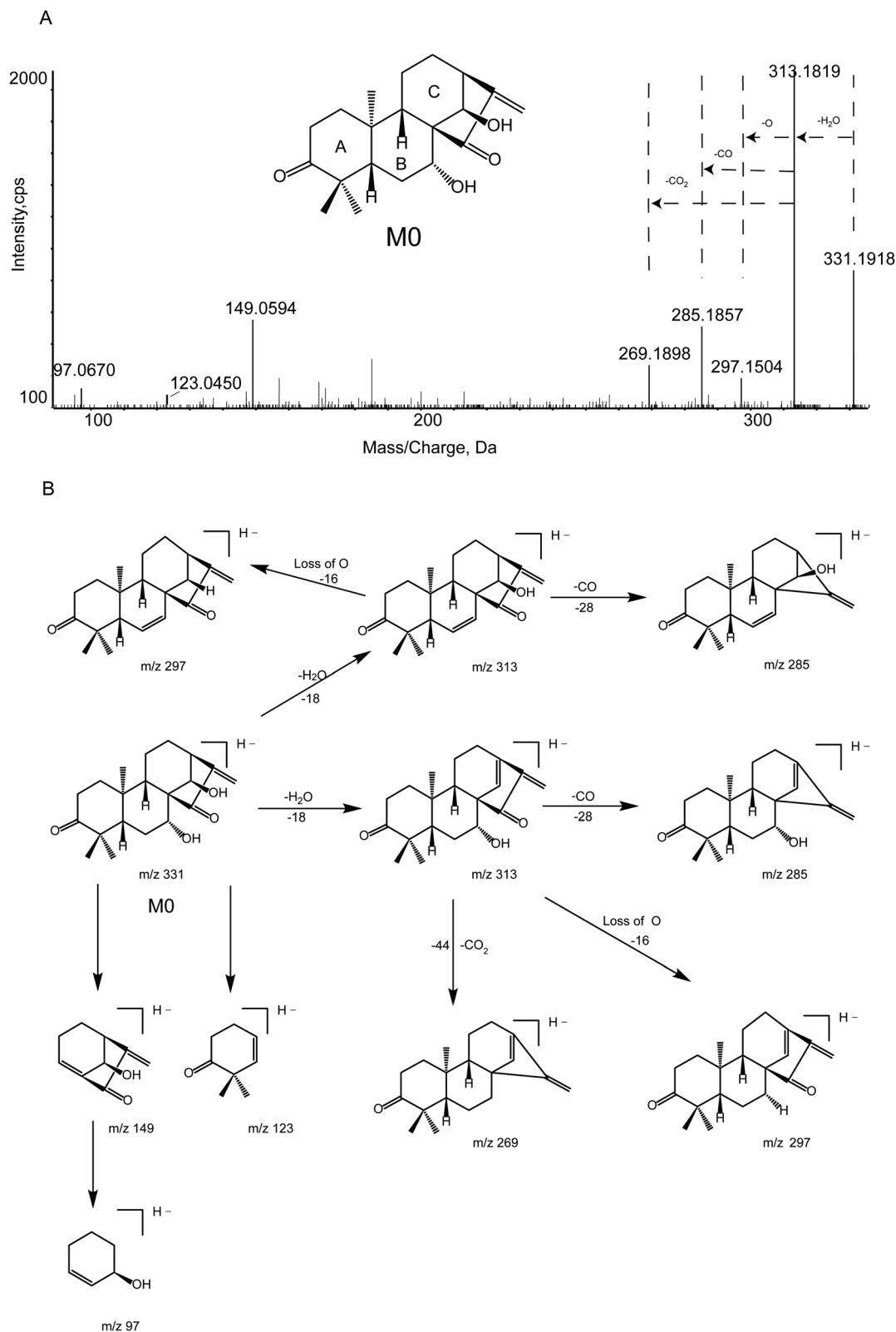

Fig. 2   The MS/MS spectrum of deprotonated GLA and its fragmentation pathway.

means of the data post-processing software MetabolitePilot™. In **M21–M23**, the deprotonated ion at m/z 345 ([M − H]⁻) successively eliminated H_2O and CO to produce characteristic products ions at m/z 327 ([M − H–H_2O]⁻) and 299 ([M − H–H_2O–CO]⁻), respectively. Afterwards, the product ion at m/z 283 ([M − H–H_2O–CO_2]⁻) was formed by the loss of CO_2. The software prompted that **M21–M23** were produced by a ketone reaction.

In **M21**, the diagnostic ions at m/z 137 and 97 were by ketogenic A ring and original C ring, respectively. Only the C-1 and C-2 positions in the A ring may undergo a ketone reaction. According to the oxidation mechanism, a site having a large electron cloud density is easily oxidized. Hence, the C-1 position was probable to undergo a ketone reaction due to a larger electron cloud density.

In **M22**, fragment ions at m/z 149 and 123 were the same as **M0**. The above information implied that the ketone was formed in the B ring. Only the C-6 was consistent.

In **M23**, the characteristic fragment ion was at m/z 163. It strongly implied that the oxidation of alkyl group to ketone group was conducted at C-11 or C-12. According to the principle of minimum energy and steric hindrance effect, the C-12 position was easier to form a ketone. The lowest energy of ketone metabolites at C-11 and C-12 were 59.3359 kcal mol⁻¹ and 59.1798 kcal mol⁻¹, respectively.

3.2.5 Metabolites *via* losing of H_2O, CO, or O. **M1** (t_R = 26.78 min) and **M2** (t_R = 27.12 min) were detected in the full-scan mass spectrum as the deprotonated ion at m/z 313 ($C_{20}H_{26}O_3$). In **M1–M2**, by losses of CO and CO_2, the distinctive product ions at m/z 285 and 269 were exhibited. Dehydration may occur at C-14 or C-7. In **M1**, fragment ion at m/z 131 suggested dehydration at C-14. In **M2**, fragment ion at m/z 149 was confirmed the fact that the C ring did not react, *i.e.*, C-7 underwent dehydration reaction.

M5 was eluted at 14.41 min. It showed the elemental composition of $C_{19}H_{28}O_3$. Fragment ions at m/z 285 and 267 were produced *via* successively losing H_2O from the deprotonated ion at m/z 303 ([M − H]⁻). Besides, characteristic fragment ion at m/z 123 was observed.

M6 (t_R = 28.53 min) and **M7** (t_R = 29.11 min) showed the elemental composition of $C_{20}H_{28}O_3$. By losses of H_2O and CO, the distinctive product ions at m/z 297 ([M − H–H_2O]⁻) and 269 ([M − H–H_2O–CO]⁻) were created by the deprotonated ion at m/z 315 ([M − H]⁻) in **M6–M7**. Besides, **M6** generated the KPIs at m/z 149, 123, and 97. **M6** was observed by the loss of an oxygen atom from C-7. As for **M7**, the product ion at m/z 253 ([M − H–H_2O–CO_2]⁻) was formed by the loss of CO_2. Fragment ion at m/z 133 was contributed to losing an oxygen atom from C14.

3.2.6 Demethylation. **M3** and **M4** were eluted at 28.08 min and 29.34 min, respectively. The elemental composition was $C_{19}H_{26}O_4$. The deprotonated ion at m/z 317 ([M − H]⁻) of **M3–M4** successively eliminated H_2O and CO to produce ions at m/z 299 ([M − H–H_2O]⁻) and 271 ([M − H–H_2O–CO]⁻), respectively. Next, the product ion at m/z 255 ([M − H–H_2O–CO_2]⁻) was formed by the loss of CO_2 from the ion at m/z 299. In the MS/MS spectrum of **M3**, KPIs at m/z 123 and 97 indicated demethylation did not perform in the A ring or C ring. In other words, the

demethylation reaction had no choice but happened at C-10. As for **M4**, KPIs were only at m/z 149 and 97. Those implied that the reaction was in the A ring at methyl group.

3.2.7 Hydrogenation. **M8**, **M9**, and **M10** ($C_{20}H_{30}O_4$) were eluted at 23.01 min, 20.13 min, and 20.43 min, respectively. They showed the same deprotonated ion at m/z 333 ([M − H]⁻). The possible hydrogenation reaction sites were at carbon–carbon double bonds at C-16, carbonyl group at C-3 and C-15 positions.

In **M8**, the deprotonated ion at m/z 333 ([M − H]⁻) successively eliminated H_2O and CO to produce ions at m/z 315 ([M − H–H_2O]⁻) and 287 ([M − H–H_2O–CO]⁻), respectively. Subsequently, the product ion at m/z 271 ([M − H–H_2O–CO_2]⁻) was formed by the loss of CO_2 from the ion at m/z 315. The fragment ion at m/z 151 was 2 Da higher than that of **M0**, which indicated that hydrogenation took place in the C rings at C16–C17. **M9** exhibited the dehydrated product ion at m/z 315 and fragment ions at m/z 151, 123 and 97. And no product ions after CO or CO_2 removal have been found, indicating that hydrogenation occurred at C-15. For **M10**, in addition to the fragment ions generated by the losses of H_2O, CO, and CO_2, fragment ions at m/z 149, 97 and 125 were also observed. The fragment ion at m/z 125 indicated that the hydrogenation occurred at the C-3 position of the A ring.

3.2.8 Internal hydrolysis. **M11** (t_R = 11.28 min) showed the molecular formula of $C_{20}H_{30}O_5$. The deprotonated ion at m/z 349 ([M − H]⁻) successively eliminated H_2O and CO to produce characteristic products ions at m/z 331 ([M − H–H_2O]⁻) and 303 ([M − H–H_2O–CO]⁻), respectively. Then, the product ion at m/z 287 ([M − H–H_2O–CO_2]⁻) was formed by the loss of CO_2 from the ion at m/z 331. The indicator ion at m/z 167 may be produced by the internal hydrolysis of the C ring at the carbon–carbon double bonds.

3.2.9 Desaturation. **M12** and **M13** ($C_{20}H_{26}O_4$) were the isomeric metabolites and eluted at 18.34 min and 18.05 min, respectively. The deprotonated ion at m/z 329 ([M − H]⁻) successively eliminated H_2O and CO to produce characteristic ions at m/z 311 ([M − H–H_2O]⁻) and 283 ([M − H–H_2O–CO]⁻), respectively. Afterwards, the product ion at m/z 267 ([M − H–H_2O–CO_2]⁻) was formed by the loss of CO_2 from the ion at m/z 311. Fragment ion of **M12** at m/z 147 suggested that the C ring lost two hydrogens. Similarly, the product ion at m/z 121 suggested that the A ring lost two hydrogens. Compounds with conjugated double bonds were more stable and were more likely to be metabolites. **M12** and **M13** were inferred underwent desaturation at C-12, C-13, and C-1, C-2, respectively.

3.2.10 Oxidation to carboxylic acid. **M14** (t_R = 24.42 min) possessed a deprotonated ion [M − H]⁻ at m/z 361. The elemental composition was $C_{20}H_{26}O_6$, 30 Da (R–CH_3 to R–COOH) higher than **M0**. The deprotonated ion at m/z 361 ([M − H]⁻) successively eliminated H_2O and CO to produce ions at m/z 343 ([M − H–H_2O]⁻) and 315 ([M − H–H_2O–CO]⁻), respectively. Then, the product ion at m/z 299 ([M − H–H_2O–CO_2]⁻) was formed by the loss of CO_2 from the ion at m/z 343. The KPIs ions at m/z 149 and 123 were observed. The above information suggested C-10 position could generate carboxylic acid metabolite.

3.2.11 Demethylation and oxidation. **M24** (t_R = 24.48 min) and **M25** (t_R = 25.25 min) exhibited the same elemental composition of $C_{19}H_{26}O_5$. They were considered as the mono-

Table 2 Identification of metabolites appeared in urine, feces, bile, plasma and rat intestinal flora[a]

Compound ID	Formula	$[M-H]^-$ (m/z)	T_R (min)	Error (ppm)	Fragment ions	Potential pathway	Clog P	RIF	U	F	B	P
M0	$C_{20}H_{28}O_4$	331.1918	13.41	0.9	331.1918, 313.1819, 297.1504, 285.1857, 269.1898, 255.1382, **149.0594, 123.0450, 97.0670**	Parent	1.8834	+	+	+	+	+
M1	$C_{20}H_{26}O_3$	313.1818	26.78	2.5	313.1818, 285.1135, 269.1193, 131.0494, **123.0441**	Loss of water	1.8972			+		
M2	$C_{20}H_{26}O_3$	313.1819	27.12	3.1	313.1819, 285.1165, 269.1205, **149.0571**	Loss of water	2.3082			+		
M3	$C_{19}H_{26}O_4$	317.1765	28.08	2.1	317.1765, 299.1813, 271.2283, 255.2118, **123.0500, 97.0686**	Demethylation	1.3644			+		
M4	$C_{19}H_{26}O_4$	317.1764	29.34	1.7	317.1764, 299.1816, 271.2292, 255.2122, **149.0538, 97.0697**	Demethylation	1.3644			+		
M5	$C_{19}H_{28}O_3$	303.1972	14.41	2.2	303.1972, 285.0737, 267.1234, **123.0498**	Loss of CO	2.3380		+			
M6	$C_{20}H_{28}O_3$	315.1973	28.53	2.2	315.1973, 297.1815, 269.0817, **149.0602, 123.0453, 96.9605**	Loss of O	2.5922		+	+	+	+
M7	$C_{20}H_{28}O_3$	315.1968	29.11	0.7	315.1968, 297.1877, 269.0833, 253.0732, 133.0302, **96.9586**	Loss of O	2.1212		+	+	+	+
M8	$C_{20}H_{30}O_4$	333.2078	23.01	1.9	333.2078, 315.1951, 287.1812, 271.1692, 151.0767, **123.0620, 96.9608**	Hydrogenation	2.2348				+	+
M9	$C_{20}H_{30}O_4$	333.2081	20.13	2.8	333.2081, 315.1960, 151.1134, **123.0510, 97.0646**	Hydrogenation	2.9720			+		
M10	$C_{20}H_{30}O_4$	333.2079	20.43	2.0	333.2079, 315.1968, 287.1327, 271.1692, **149.0671, 125.0961, 96.9600**	Hydrogenation	2.2854			+		
M11	$C_{20}H_{30}O_5$	349.2020	11.23	−0.2	349.2020, 331.1912, 303.1963, 287.2022, 167.1065, **96.9607**	Internal hydrolysis	1.0482	+	+			
M12	$C_{20}H_{26}O_4$	329.1760	18.34	0.5	329.1760, 311.0892, 283.1180, 267.1007, 147.0371, **123.0451**	Desaturation	1.6594		+	+	+	
M13	$C_{20}H_{26}O_4$	329.1765	18.05	1.8	329.1765, 311.2208, 283.2639, 267.1934, **149.0601, 121.0364**	Desaturation	1.7394		+	+	+	
M14	$C_{20}H_{26}O_6$	361.1657	24.42	0.1	361.1657, 343.1899, 315.1971, 299.2137, **149.0595, 123.0509**	Oxidation to carboxylic acid	0.6694	+	+			*
M15	$C_{20}H_{28}O_5$	347.1866	3.01	0.6	347.1866, 329.1686, 301.1778, 285.1866, **149.0674, 123.0623**	Mono-oxidation	1.1712		+	+	+	
M16	$C_{20}H_{28}O_5$	347.1874	4.02	2.8	347.1874, 329.2308, 301.1415, 285.1857, 165.1280, 147.0799	Mono-oxidation	1.8424		+	+	+	
M17	$C_{20}H_{28}O_5$	347.1859	22.25	−1.4	347.1859, 329.1782, 301.2046, 285.1864, **149.0619, 139.0721**	Mono-oxidation	0.5968		+	+	+	
M18	$C_{20}H_{28}O_6$	363.1821	11.62	2.1	363.1821, 345.1675, 317.2071, 301.1773, 165.0883	Di-oxidation	0.5558	+	+	+		
M19	$C_{20}H_{28}O_6$	363.1826	13.25	3.7	363.1821, 345.1675, 317.2073, 301.1771, 165.0882	Di-oxidation	1.1302	+	+	+		
M20	$C_{20}H_{28}O_7$	379.1753	23.14	−2.6	379.1753, 361.2113, 333.2042, 317.1679, 165.1244, 139.1135	Tri-oxidation	−1.5640		+	+		*
M21	$C_{20}H_{28}O_7$	345.1701	7.98	−1.9	345.1701, 327.2164, 299.1661, 283.1735, 137.0965, **97.0653**	Ketone formation	1.2740		+		+	
M22	$C_{20}H_{26}O_5$	345.1704	8.23	−1.0	345.1704, 327.2086, 299.1842, 283.0953, **149.0611, 123.0445**	Ketone formation	0.4673		+		+	
M23	$C_{20}H_{26}O_5$	345.1702	8.44	−1.6	345.1717, 327.2098, 299.1796, 283.1672, 163.0760	Ketone formation	1.0298		+		+	
M24	$C_{19}H_{26}O_5$	333.1689	24.48	−5.4	333.1689, 315.1580, 287.1633, 271.1687, 165.0540, **123.0457**	Demethylation and oxidation	1.3223		+			
M25	$C_{20}H_{26}O_5$	333.1691	25.25	−4.9	333.1691, 315.1671, 287.1503, 271.1730, 165.0931, 107.0431	Demethylation and oxidation	1.3234		+			
M26	$C_{19}H_{26}O_6$	349.1632	8.62	−6.0	349.1636, 331.1516, 303.1963, 287.1991	Demethylation and di-oxidation	−0.6344			+		
M27	$C_{19}H_{26}O_6$	349.1636	8.74	−5.8	349.1636, 331.1516, 303.1963, 287.1991	Demethylation and di-oxidation	0.0368			+		
M28	$C_{19}H_{26}O_6$	349.1650	8.83	−1.9	349.1636, 331.1516, 303.1963, 287.1991	Demethylation and di-oxidation	0.6112			+		

Table 2 (Contd.)

Compound ID	Formula	$[M - H]^-$ (m/z)	T_R (min)	Error (ppm)	Fragment ions	Potential pathway	Clog P	RIF	U	F	B	P
M29	$C_{19}H_{28}O_4$	319.1910	12.21	−1.5	319.1913, 301.1800, 273.1723, 257.1903, 151.0537	Demethylation and hydrogenation	1.7158		+		+	
M30	$C_{19}H_{28}O_4$	319.1913	12.44	−0.4	319.1913, 301.1800, 273.1723, 257.1903, 151.0537	Demethylation and hydrogenation	1.7158		+		+	
M31	$C_{20}H_{30}O_6$	365.1962	18.90	−2.1	365.1962, 347.1867, 319.1932, 303.1956, 167.0678, **149.0620, 123.0446**	Oxidation and internal hydrolysis	0.3359		+	+		
M32	$C_{20}H_{30}O_7$	381.1920	13.25	0.2	381.1920, 363.1791, 335.1438, 319.1531, 167.0665, **149.0613, 139.0387, 123.0436**	Di-oxidation and internal hydrolysis	−0.9506	+	+	+		
M33	$C_{21}H_{30}O_4$	345.2100	18.92	1.7	345.2100, 327.1601, 299.1634, 283.1699, 163.0399, **123.0439**	Methylation	2.0116	+				
M34	$C_{21}H_{30}O_4$	345.2101	19.87	1.7	345.2101, 327.1600, 299.1647, 283.1673, **149.0599**	Methylation	1.9848	+				
M35	$C_{20}H_{28}O_7S$	411.1499	5.62	3.9	411.1499, 393.1781, 365.1366, 349.1960, 229.0632, **123.0420, 97.0665**	Sulfate conjugation	1.1902		+			*
M36	$C_{20}H_{28}O_7S$	411.1490	5.75	1.6	411.1490, 393.1571, 365.2022, 349.1958, **149.0594, 123.0556**	Sulfate conjugation	1.1812		+			
M37	$C_{20}H_{28}O_8S$	427.1424	10.66	−2.0	427.1424, 409.2193, 381.1955, 365.2184, 165.0637, **123.0519**	Oxidation and sulfate conjugation	1.1402			+		
M38	$C_{26}H_{38}O_9$	493.2049	9.87	−6.2	493.2049, 475.2261, 447.2853, 175.0731, **149.0589, 123.0546**	Demethylation and glucuronide conjugation	−0.6910		+			*
Total								7	25	18	17	7

[a] RIF: rat intestinal flora; U: urine; F: feces; B: bile; P: plasma. Total: total metabolites. KPIs were indicated in bold face. "+": the MS data detected by DDA and DIA. "*": the MS data only detected by DIA. The MS/MS fragment data of **M1**, **M2**, **M8**, **M9**, **M10** could only be observed under DDA mode.

oxidized product of demethylated **M0**. The deprotonated ion at m/z 333 ($[M - H]^-$) successively eliminated H_2O and CO to produce ions at m/z 315 ($[M - H–H_2O]^-$) and 287 ($[M - H–H_2O–CO]^-$), respectively. Afterwards, the product ion at m/z 271 ($[M - H–H_2O–CO_2]^-$) was formed by the loss of CO_2 from the ion at m/z 315. In **M24**, the fragment ion at m/z 165 suggested that the C ring was oxidized while the ion at m/z 123 revealed that demethylation was not connected to the A ring. Namely, the demethylation reaction occurred at C-10. In **M25**, the characteristic fragment ions at m/z 165 and 107 indicated that the C ring was oxidized while C-4 position experienced demethylation. According to the oxidation reaction theory, the 13-position of the C ring was easily oxidized.

3.2.12 Demethylation and di-oxidation. Metabolites **M26**, **M27**, and **M28** ($C_{20}H_{26}O_6$) appeared as deprotonated molecular ion $[M - H]^-$ at m/z 349, together with the retention time of 8.62 min, 8.74 min and 8.83 min, respectively. The deprotonated ion at m/z 349 ($[M - H]^-$) successively eliminated H_2O and CO to produce ions at m/z 331 ($[M - H–H_2O]^-$) and 303 ($[M - H–H_2O–CO]^-$), respectively. Then, the product ion at m/z 287 ($[M - H–H_2O–CO_2]^-$) was formed by the loss of CO_2 from the ion at m/z 331. Referring to 3.2.2 and 3.2.6, there were 6 possible metabolites. The C-4 or C-10 position was demethylated, accompanied by a di-oxidation reaction at C-1 and C-6, or C-1 and C-13 or C-6 and C-13. The minimize energy values were 61.1376 kcal mol^{-1}, 41.9139 kcal mol^{-1}, 55.1313 kcal mol^{-1}, 48.7821 kcal mol^{-1}, 47.0962 kcal mol^{-1}, and 41.9140 kcal mol^{-1}, respectively. Hence, demethylation occurred at the C-4 or C-10

position, while oxidation occurred at C-1 and C-13 positions, or demethylation at the C10 position, while the C-6 and C-13 positions were oxidized. Moreover, the Clog P values of them displayed 0367, 0.0368 and 0.6112, respectively. Based on the above information, **M26**, **M27**, and **M28** were temporarily deduced.

3.2.13 Demethylation and hydrogenation. Metabolites **M29** and **M30** ($C_{19}H_{28}O_4$) were the isomeric metabolites with the deprotonated ($[M - H]^-$) ion at m/z 319, which were eluted at 12.21 min and 12.44 min, respectively. The deprotonated ion at m/z 319 ($[M - H]^-$) of **M29–M30** successively eliminated H_2O and CO to produce characteristic products ions at m/z 301 ($[M - H–H_2O]^-$) and 273 ($[M - H–H_2O–CO]^-$), respectively. Then, the product ion at m/z 257 ($[M - H–H_2O–CO_2]^-$) was formed by the loss of CO_2 from the ion at m/z 301. The fragment ion at m/z 151 was 2 Da higher than that of **M0**, which indicated that hydrogenation took place in the C ring at C16–C17. In addition, demethylation was connected to the C-4 and C-10 positions. Compounds can be distinguished by the Clog P values.

3.2.14 Oxidation and internal hydrolysis. M31 was eluted at 18.90 min, showing the elemental composition of $C_{20}H_{30}O_7$, 34 Da (H_2O_2) higher than **M0**. The deprotonated ion at m/z 365 ($[M - H]^-$) successively eliminated H_2O and CO to produce characteristic products ions at m/z 347 ($[M - H–H_2O]^-$) and 319 ($[M - H–H_2O–CO]^-$), respectively. Subsequently, the product ion at m/z 303 ($[M - H–H_2O–CO_2]^-$) was formed by the loss of CO_2 from the ion at m/z 347. The typical ion was at m/z 167, implying that the C ring was added water on the carbon–carbon

double bonds. The oxidation reaction was inferred in the B ring at C-6 *via* the presence of fragment ions at m/z 123 and 149.

3.2.15 Di-oxidation and internal hydrolysis. M32 (t_R = 13.25 min) possessed a deprotonated ion $[M − H]^-$ at m/z 381. The elemental composition was $C_{20}H_{30}O_7$, 50 Da (H_2O_3) higher than **M0**. The deprotonated ion at m/z 381 ($[M − H]^-$) successively eliminated H_2O and CO to produce characteristic products ions at m/z 363 ($[M − H–H_2O]^-$) and 335 ($[M − H–H_2O–CO]^-$), respectively. Afterwards, the product ion at m/z 319 ($[M − H–H_2O–CO_2]^-$) was formed by the loss of CO_2 from the ion at m/z 363. The characteristic ion at m/z 167 implied that the C ring

carbon–carbon double bonds were added water. Fragment ions at m/z 139, 149 and 123 implied that one of the oxidation reactions occurred in the A ring and the other oxidation reaction happened in the B ring. The most likely sites were at C-1 and C-6.

3.3 Phase II metabolites identification

Metabolic profile involved methylation conjugation, sulfate conjugation, and glucuronide conjugation. Products that have undergone both phase I metabolism and phase II metabolism have also been observed.
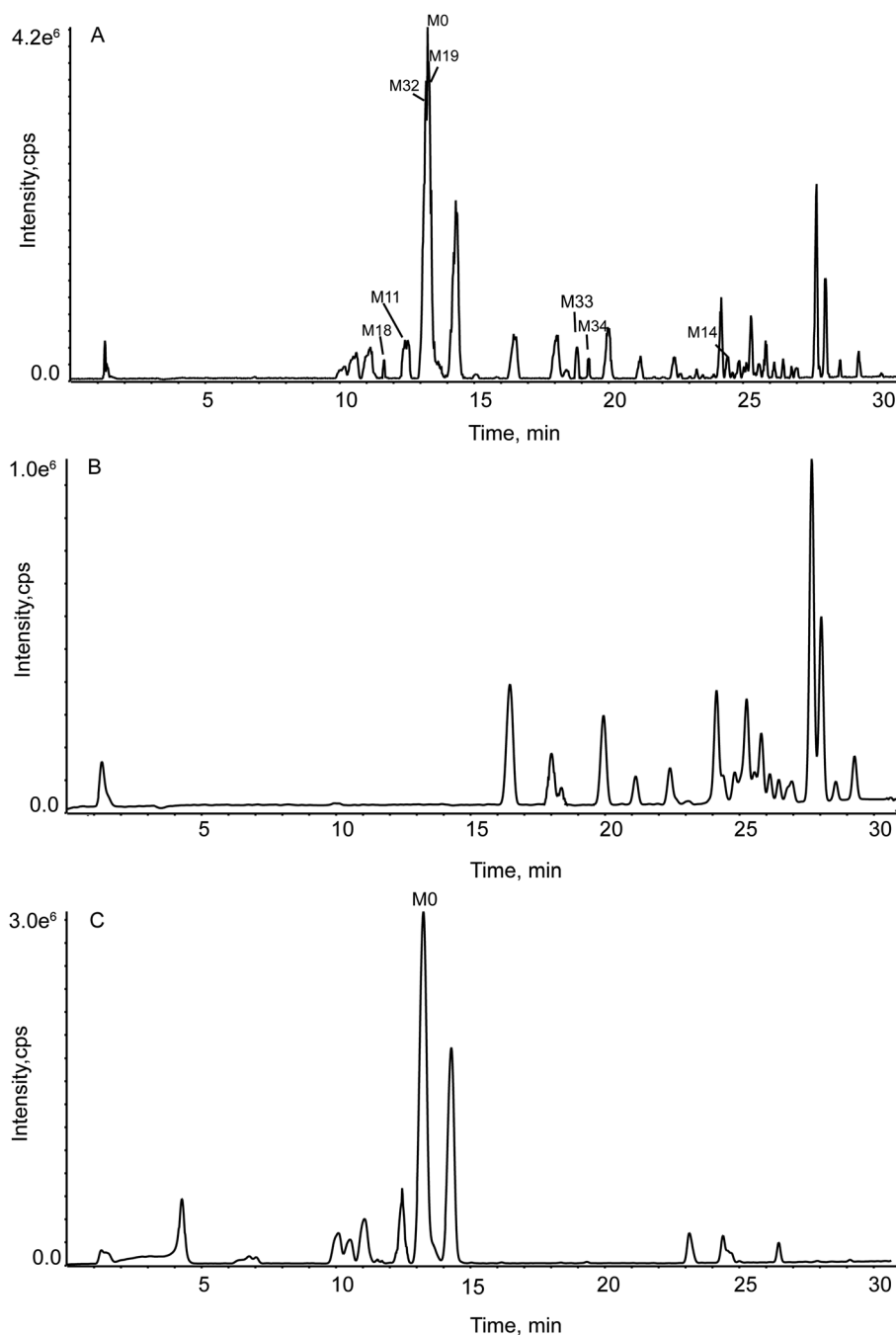
Fig. 3 TIC for the group *in vitro* by DDA. (Panel A: the RIF sample group; Panel B: blank B group; Panel C: blank C group.)

3.3.1 Methylation. Metabolites **M33** and **M34** ($C_{21}H_{30}O_4$) with deprotonated molecular ions $[M - H]^-$ at m/z 345 were eluted at 18.92 min and 19.87 min, respectively. It was likely that two sites of C-7 and C-14 were underwent methylation. In **M33**, the deprotonated ion at m/z 345 ($[M - H]^-$) successively eliminated H_2O and CO to produce characteristic products ions at m/z
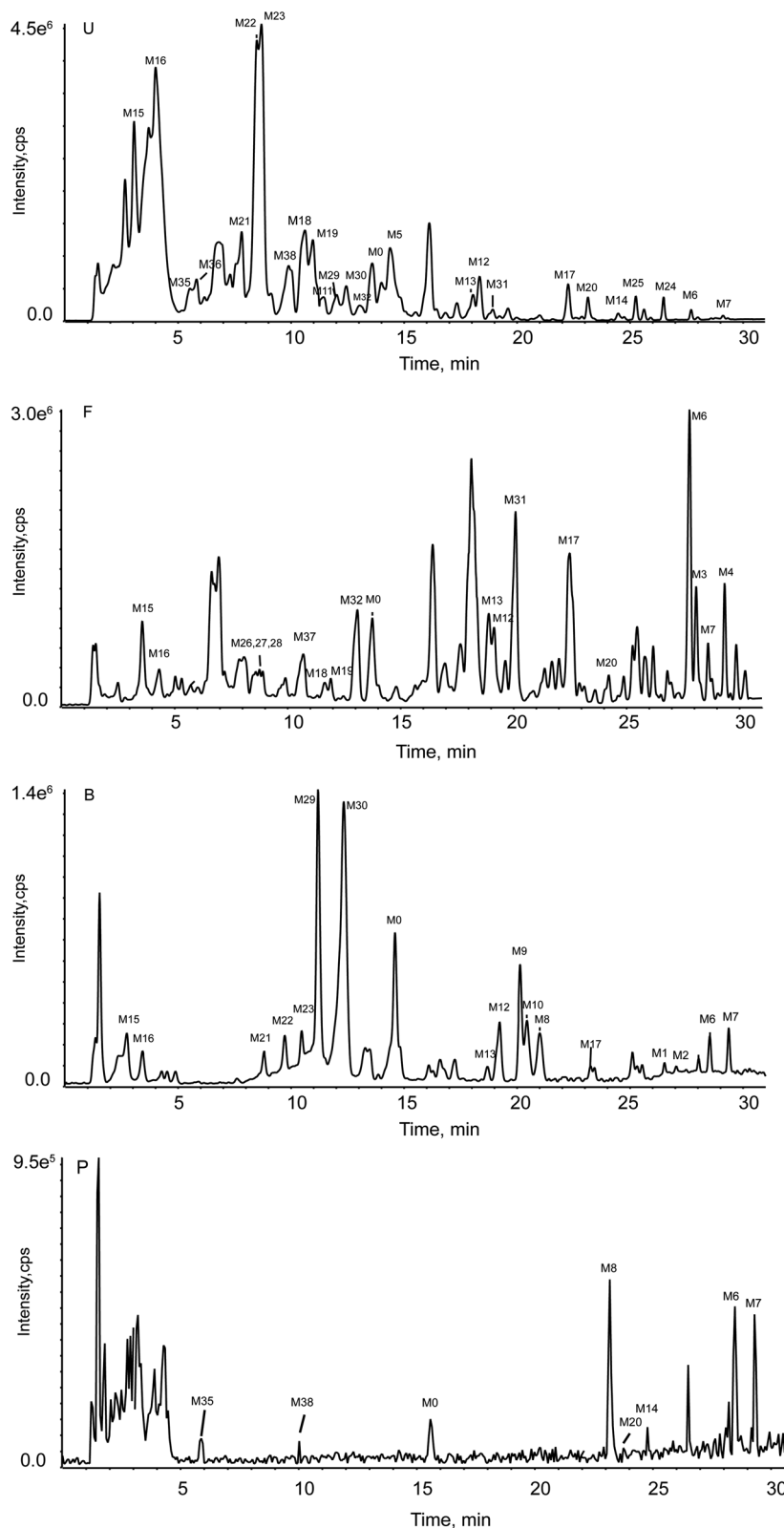

Fig. 4 TIC for the experimental group *in vivo*. (Panel U: the group in urine by DDA; Panel F: the group in feces by DDA; Panel B: the group in bile by DDA; Panel P: the group in plasma by DIA.)

327 ([M − H–H_2O]$^-$) and 299 ([M − H–H_2O–CO]$^-$), respectively. Subsequently, the product ion at m/z 283 ([M − H–H_2O–CO_2]$^-$) was formed by the loss of CO_2 from the ion at m/z 327. The characteristic ion at m/z 163 implied the C ring was methylated. As for **M34**, distinctive product ions were also detected by eliminating H_2O, CO, and CO_2. The ion at m/z 149 indicated that the methylation reaction was not connected to A ring. In other words, methylation occurred at the C-7 position of **M34**.

3.3.2 Sulfate conjugation. **M35** and **M36** were successively eluted at 5.62 min and 5.75 min and were isomers of $C_{20}H_{28}O_7S$,

80 Da (SO_3) higher than **M0**. In **M35**, the deprotonated ion at m/z 411 ([M − H]$^-$) successively eliminated H_2O and CO to produce ions at m/z 393 ([M − H–H_2O]$^-$) and 365 ([M − H–H_2O–CO]$^-$), respectively. Next, the product ion at m/z 349 ([M − H–H_2O–CO_2]$^-$) was formed by the loss of CO_2 from the ion at m/z 393. The fragment ion at m/z 229 was 80 Da higher than 149, indicating that sulfate conjugation occurred at C-14. **M36** exhibited debris ions at m/z 411, 393, 365, 349, 149, and 123. These indicated that sulfate conjugation occurred at C-7.
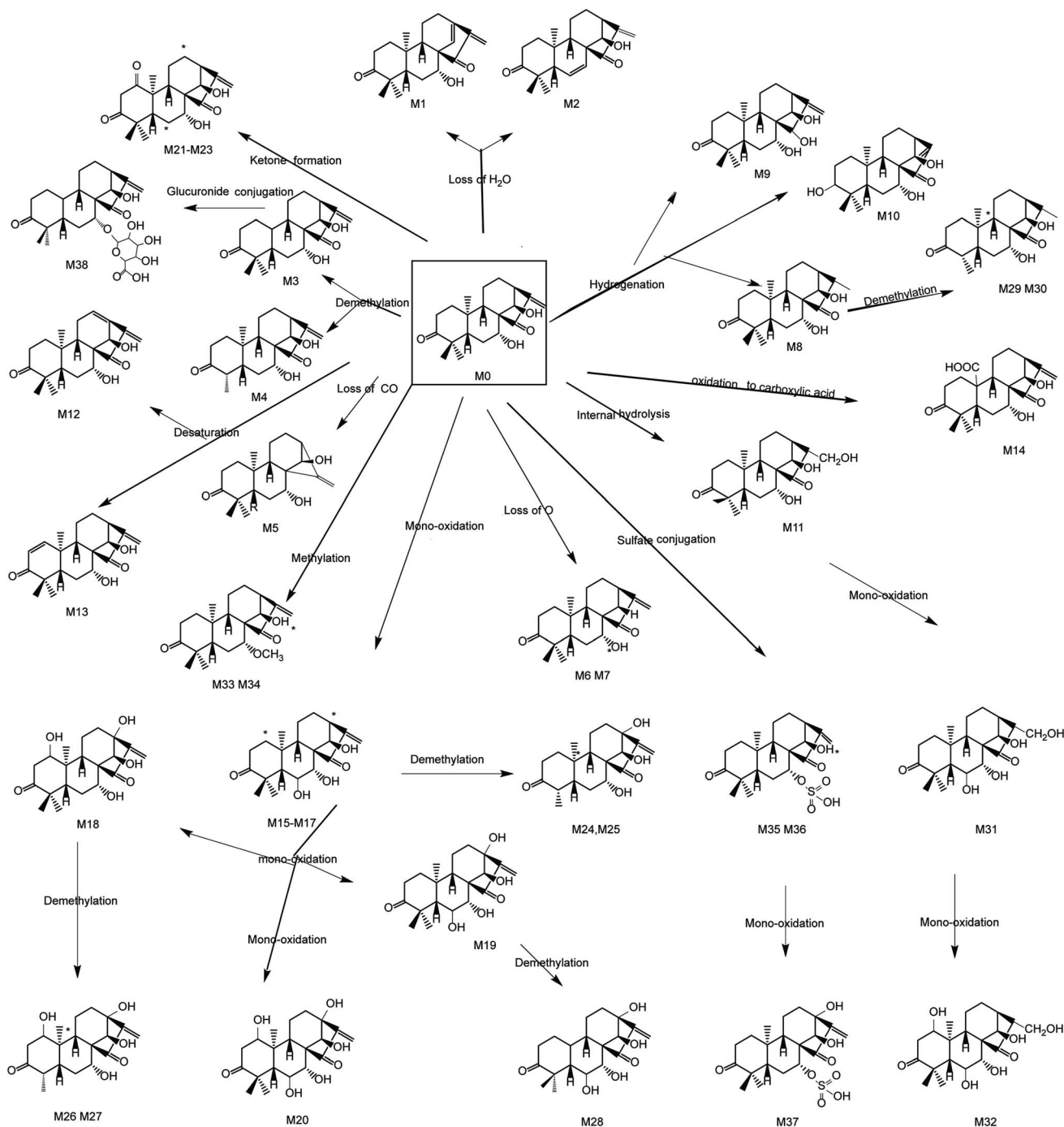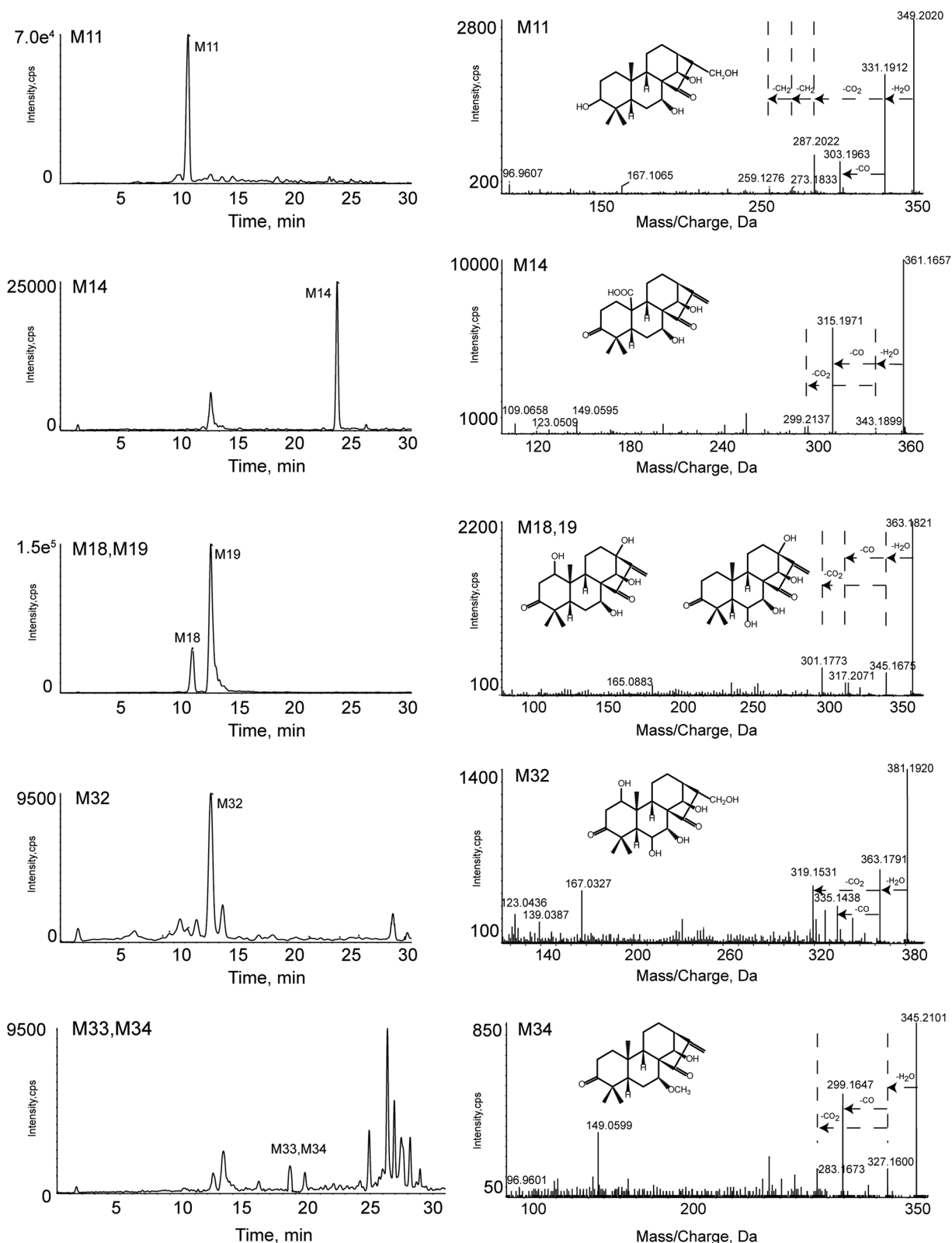

Fig. 5 The proposed GLA metabolic profiles *in vitro* and *in vivo*.

3.3.3 Oxidation and sulfate conjugation. M37 (t_R = 10.66 min) possessed a deprotonated ion at m/z 427 with the elemental composition of $C_{20}H_{28}O_8S$, 96 Da (SO_4) higher than **M0.** The deprotonated ion at m/z 427 ([M − H]⁻) successively eliminated H_2O and CO to produce ions at m/z 409 ([M − H–H_2O]⁻) and 381 ([M − H–H_2O–CO]⁻), respectively. Then, the

Fig. 6 The EIC and MS/MS spectra of metabolites *in vitro*, including **M11, M14, M18, M19, M32, M33, M34**.

product ion at m/z 365 ([M − H–H_2O–CO_2]⁻) was formed by the loss of CO_2 from the ion at m/z 409. Diagnostic ions at m/z 165 and 123 suggested that sulfate conjugation occurred at C-7 and mono-oxidation occurred at C-13.

3.3.4 Demethylation and glucuronide conjugation. M38

was eluted at 9.87 min with the molecular formula of $C_{26}H_{38}O_9$ ([M − H]⁻ m/z 493), 162 Da higher than **M0**. The deprotonated ion at m/z 493 ([M − H]⁻) successively eliminated H_2O and CO to produce ions at m/z 475 ([M − H–H_2O]⁻) and 447 ([M − H–H_2O–CO]⁻), respectively. The characteristic ion of glucuronic acid was at m/z 175. Fragment ions at m/z 149, 123 implied that demethylation occurred at C-10 and glucuronic conjugation occurred at C-7.

3.4 Comparison of metabolites acquired by DDA and DIA

There is almost no difference in the type and amount of metabolites obtained by the DDA or DIA method in rat urine, feces, bile, and RIF. But in plasma, the results obtained by these two acquisition modes varied widely. Specifically, 3 and 7 metabolites were detected by DDA and DIA, respectively (see Fig. 8). However, for some compounds (**M1, M2, M8, M9, M10**), the corresponding MS/MS fragment data could only be detected *via* DDA mode. Previous research has shown that matrix effects might have failed in MS/MS data acquisition in DIA mode.[31] Based on the complementarity of DDA and DIA modes, the hit
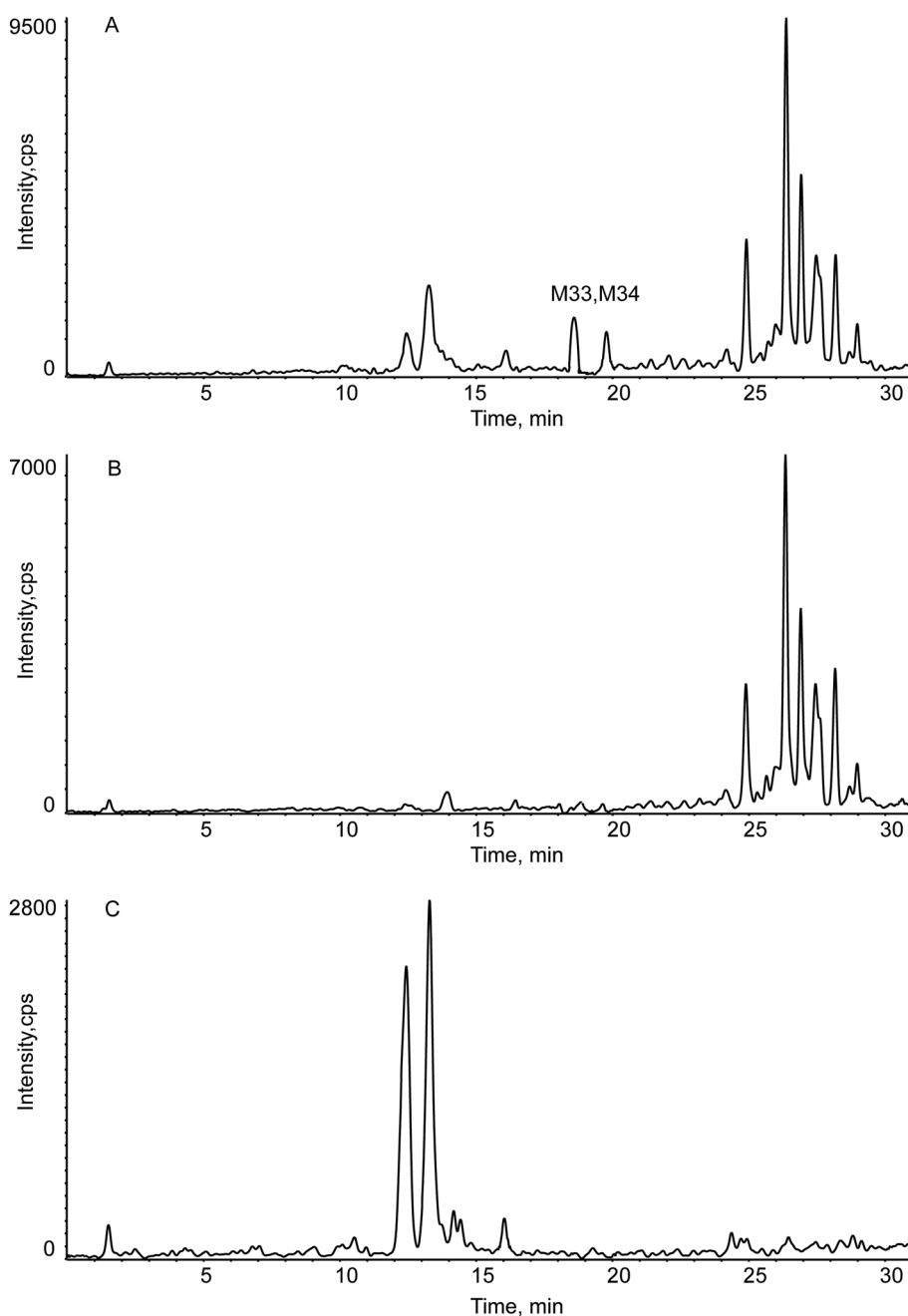

Fig. 7   The EIC of **M33**, **M34** *in vitro* (Panel A: the RIF sample group; Panel B: blank B group; Panel C: blank C group).

rate of identifying trace metabolites was superbly increased, thereby enriching metabolic profile.

3.5 Metabolic profile of GLA

The characteristic metabolic profiles of phase I were oxidation, demethylation, hydrogenation, internal hydrolysis, desaturation, and ketone formation. Methylation conjugation, sulfate conjugation, oxidation and sulfate conjugation, and glucuronide conjugation were metabolic routes of phase II. Furthermore, GLA distinctively underwent successional oxidation and demethylation reaction. This is extremely evident in the metabolic profile. The possible metabolic profiles of GLA *in vitro* and *in vivo* were displayed in Fig. 5. Besides, Table 2 was the identification of metabolites that appeared.

3.6 Two blank groups for RIF experiment

By consulting the literature, we found that not a few rat intestinal flora hatching experiments only set up one blank group. Such a design was very unscientific and untrustworthy. In the study, two blank groups were applied.

The Fig. 3(A) stood for rat intestinal flora (RIF) experimental group (100 μL GLA in culture medium fluid). To exclude the interference of other substances, we compared the RIF sample chromatogram with two blanks. The Fig. 3(B) stood for the blank B sample and the Fig. 3(C) stood for blank C sample. The blank B (100 μL methanol in culture medium fluid) was to eliminate the effects of solvents on metabolism. The blank C (100 μL GLA in anaerobic medium fluid) was to investigate whether there was a decomposition of the drug caused by non-intestinal flora in the anaerobic culture solution. By comparing the A, B, and C, the substances presented in the A but not in the B and C were truly caused by the action of RIF.

3.7 Comparison of metabolites *in vitro* and *in vivo*

Drug metabolism is an essential part of pharmacological mechanisms, pharmacokinetics research, new drug screening, and clinical application. In the study, we preliminary studied the metabolism *in vivo* (plasma, urine, bile, and faces) and *in vitro* (rat intestinal flora) in this work. A total of 38 metabolites *in vivo* while 7 metabolites *in vitro* were temporarily recognized. Moreover, 5 metabolites *in vitro* were also found *in vivo*, two methylation metabolites were only found *in vitro*. The above information suggested that the metabolism *in vivo* and *in vitro* had a huge difference in some ways. Based on the metabolite
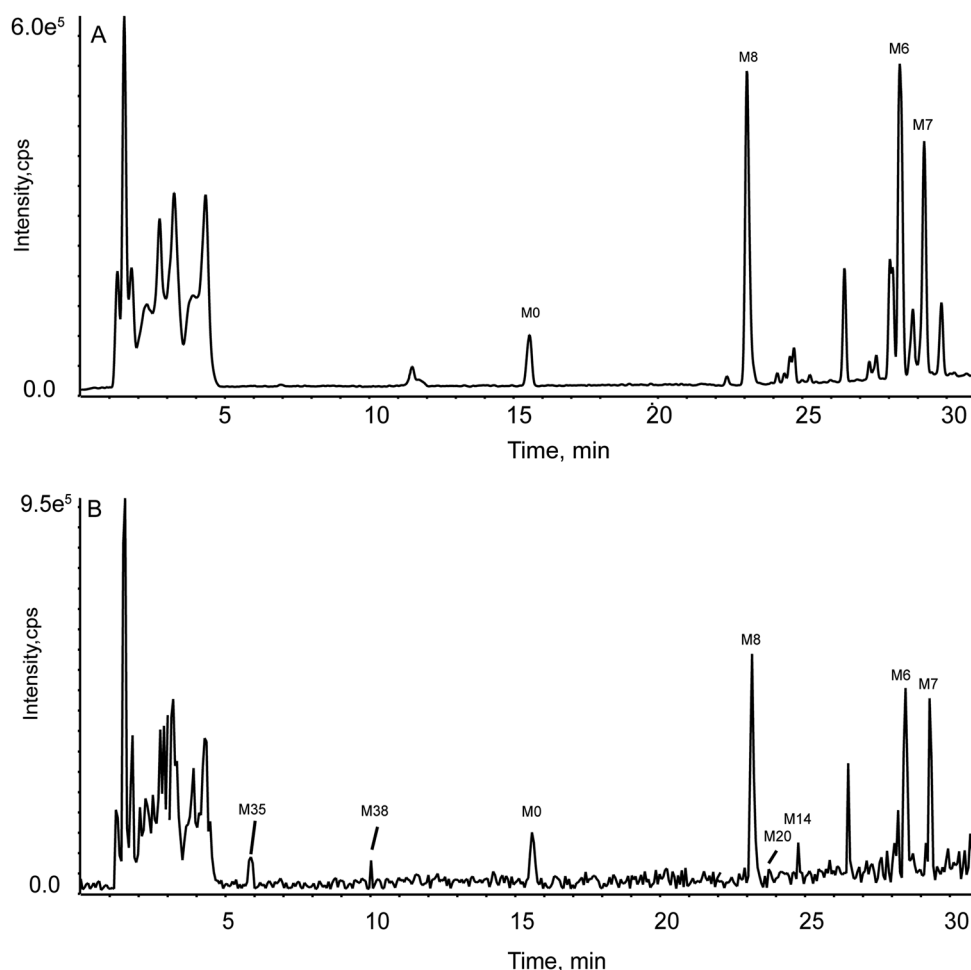

Fig. 8 TIC for the experimental group in rat plasma by two acquisitions. (Panel A: by DDA mode; Panel B: by DIA mode.)

observed, this is important to further research on what enzymes may have played a role. After all, enzymes are the driving force for metabolism but it is very complicated.

The total ion chromatogram (TIC) for the experimental sample group *in vitro* was shown in Fig. 3(A). Fig. 4 stands for TIC for the experimental sample groups *in vivo*.

The EIC and MS/MS spectra of metabolites *in vitro* were showed in Fig. 6. But the EIC of **M33**, **M34** ($C_{21}H_{30}O_4$) has many interfering substances. For a clear expression on how we got the metabolites, we introduced Fig. 7. The A, B, and C represented the experimental sample group, blank B, blank C, respectively. The EIC presented in A, but not presented in B and C were the metabolites.

4. Conclusions

By this novel metabolite identification strategy, 32 phase I metabolites and 6 phase II metabolites were temporarily identified *in vitro* and *in vivo*, 25, 18, 17 and 11 in rat urine, feces, bile, and plasma included, respectively. Besides, a total of 7 metabolites were detected under the action of intestinal flora. Characteristic metabolic profiles of phase I were oxidation, demethylation, hydrogenation, internal hydrolysis, desaturation, and ketone formation. Methylation, sulfate conjugation, oxidation and sulfate conjugation, and glucuronide conjugation belonged to metabolic routes of phase II. Regrettably, due to the trace amount of metabolic production, we cannot use nuclear magnetics for structural confirmation. Certainly, the role of these metabolites in human life activities requires further research. In a word, this study based on an innovative research strategy not only provided a reference for further study of the pharmacology and mechanism of GLA but also some value for studies of other ent-kauranoid diterpenoids even other herbs.

Abbreviations

UHPLC-Q-TOF-MS/MS	Ultra high performance liquid chromatography coupled with hybrid triple quadrupole time-of-flight mass spectrometry
GLA	Glaucocalyxin A
DDA	Data-dependent acquisition
DIA	Data-independent acquisition
KPIs	Key product ions
PCVG	Principal component variable grouping filter
DBS	Dynamic background subtraction
MMDF	Multiple mass defect filtering
MDF	Mass defect filter
EIC	Extracted ion chromatogram
TIC	Total ion chromatogram
PIF	Product ion filter
NLF	Neutral loss filtering
CMC-Na	Sodium carboxymethyl cellulose
RIF	Rat intestinal flora

Conflicts of interest

The authors declare no conflict of interest.

Acknowledgements

References

1 Nanjing University of Chinese Medicine, *HBR's 10 Must Reads on Managing Yourself*, Shanghai Scientific & Technical Press, Shanghai, 2014, p. 2040.

2 W. Huang, X. Guan and Y. Lv, Simultaneous determination of glaucocalyxin A and glaucocalyxin B in rat plasma by LC-MS/MS and its application to a pharmacokinetic study after oral administration of Rabdosia japonica extract, *Biomed. Chromatogr.*, 2018, **32**, 4089.

3 S. Han, X. Sheng and B. Quan, Diterpenoids from Isodon species and their biological activities, *Nat. Prod. Rep.*, 2006, **23**, 673–698.

4 S. Hong, S. Lee, X. Han, C. Lee and D. Lee, Ent-kaurane diterpenoids from Isodon japonicus, *J. Nat. Prod.*, 2008, **71**, 1055–1058.

5 Z. Xiang, Y. Xu, Y. Shen, L. Jin, H. Wang and H. Chen, Diterpenoids from Rabdosia japonica, *Asian J. Chem.*, 2009, **21**, 2721–2725.

6 L. Gao, J. Zhang, W. Yang, B. Wang and J. Wang, Glaucocalyxin A induces apoptosis in human leukemia HL-60 cells through mitochondria-mediated death pathway, *Toxicol. In Vitro*, 2011, **25**, 51–63.

7 B. W. Kim, S. Koppula and S. S. Hong, Regulation of Microglia Activity by Glaucocalyxin-A: Attenuation of Lipopolysaccharide-Stimulated Neuroinflammation through NF-kappa B and p38 MAPK Signaling Pathways, *PLoS One*, 2013, **8**, 1–11.

8 X. Xiao, W. Cao, X. Jiang, W. Zhang, Y. Zhang, B. Liu, J. Cheng, H. Huang, J. Huo and X. Zhang, Glaucocalyxin A, a negative Akt regulator, specifically induces apoptosis in human brain glioblastoma U87MG cells, *Acta Biochim. Biophys. Sin.*, 2013, **45**, 946–952.

9 L. Tang, X. Jin, X. Hu, Z. Liu and L. Yu, Glaucocalyxin A inhibits the growth of liver cancer Focus and SMMC-7721 cells, *Oncol. Lett.*, 2016, **11**, 1173–1178.

10 M. Mao, T. Zhang, Z. Wang, H. Wang, J. Xu, F. Yin, G. Wang, M. Sun, Z. Wang, Y. Hua and Z. Cai, Glaucocalyxin A-induced oxidative stress inhibits the activation of STAT3 signaling pathway and suppresses osteosarcoma progression *in vitro* and *in vivo*, *BBA, Mol. Basis Dis.*, 2019, **1865**, 1214–1225.

11 Q. Su and Y. Zhang, Glaucocalyxin A attenuates angiotensin II-induced cardiac fibrosis in cardiac fibroblasts, *Biochem. Biophys. Res. Commun.*, 2018, **503**, 1949–1954.

12 W. Li, X. Tang, W. Yi, Q. Li, L. Ren, X. Liu, C. Chu, O. Yukio, J. Zhang and L. Zhu, Glaucocalyxin A inhibits platelet activation and thrombus formation preferentially via GPVI signaling pathway, *PLoS One*, 2013, **8**, e85120.

13 Z. Xiang, X. Wu, X. Liu and Y. Jin, Glaucocalyxin A: a review, *Nat. Prod. Res.*, 2014, **28**, 2221–2236.

14 T. Zhou, J. Zhuang, Z. Wang, Y. Zhou, W. Li, Z. Wang and Z. Zhu, Glaucocalyxin A as a natural product increases amyloid β clearance and decreases tau phosphorylation involving the mammalian target of rapamycin signaling pathway, *Neuroreport*, 2019, **30**, 310–316.

15 L. Cao, Z. Chen, Y. Li, Y. Ma and R. Jin, Research RP-HPLC determination of glaucocalyxin A in rat plasma and its pharmacokinetic and excretion, *Chin. J. Pharm. Anal.*, 2006, **26**, 1534–1537.

16 L. Cao, Y. Li, Z. Chen and Y. Li, The metabolic study of glaucocalyxin A in rat *in vivo* and *in vitro*, West China, *J. Pharm. Sci.*, 2006, **21**(3), 227–229.

17 M. Zhao, L. Du, J. Tao, D. Qian, J. Guo, S. Jiang, E. Shang, J. Duan and C. Wu, Ultra-performance liquid chromatography coupled with quadrupole time-of-flight mass spectrometry for rapid analysis of the metabolites of morroniside produced by human intestinal bacteria, *J. Chromatogr. B: Anal. Technol. Biomed. Life Sci.*, 2015, **976**, 61–67.

18 Y. Li, G. Zhou, Y. Peng, P. Tu and X. Li, Screening and identification of three typical phenylethanoid glycosides metabolites from Cistanches Herba by human intestinal flora using UPLC/Q-TOF-MS, *J. Pharm. Biomed. Anal.*, 2016, **118**, 167–176.

19 Z. Huang, Y. Xu, Q. Wang and X. Gao, Metabolism and mutual biotransformations of anthraquinones and anthrones in rhubarb by human intestinal flora using UPLC-Q-TOF/MS, *J. Chromatogr. B: Anal. Technol. Biomed. Life Sci.*, 2019, **1104**, 59–66.

20 Y. Sun, L. Li, M. Liao, M. Su, C. Wan, L. Zhang and H. Zhang, A systematic data acquisition and mining strategy for chemical profiling of Aster tataricus rhizoma (Ziwan) by UHPLC-Q-TOF-MS and the corresponding anti-depressive activity screening, *J. Pharm. Biomed. Anal.*, 2018, **154**, 216–226.

21 W. W. Xie, Y. R. Jin, L. D. Hou, Y. H. Ma, H. J. Xu, K. R. Zhang, L. T. Zhang and Y. F. Du, A practical strategy for the characterization of ponicidin metabolites *in vivo* and *in vitro* by UHPLC-Q-TOF-MS based on nontargeted SWATH data acquisition, *J. Pharm. Biomed. Anal.*, 2017, **145**, 865–878.

22 X. Feng, Y. Li, C. Guang, M. Qiao, T. Wang, L. Chai and F. Qiu, Characterization of the *in vivo* and *in vitro* Metabolites of Linarin in Rat Biosamples and Intestinal Flora Using Ultra-High Performance Liquid

Chromatography Coupled with Quadrupole Time-of-Flight Tandem Mass Spectrometry, *Molecules*, 2018, **23**, 2140.

23 Y. T. Chen, X. Feng, L. Y. Li, X. Zhang, K. Song, X. P. Diao, Y. P. Sun and L. T. Zhang, UHPLC-Q-TOF-MS/MS method based on four-step strategy for metabolites of hinokiflavone *in vivo* and *in vitro*, *J. Pharm. Biomed. Anal.*, 2019, **169**, 19–29.

24 F. R. Cao, L. Feng, L. H. Ye, L. S. Wang, B. X. Xiao, X. Tao and Q. Chang, Ganoderic Acid A Metabolites and their Metabolic Kinetics, *Front. Pharmacol.*, 2017, **8**, 101.

25 T. T. Tian, Y. R. Jin, Y. H. Ma, W. W. Xie, H. J. Xu, K. R. Zhang, L. T. Zhang and Y. F. Du, Identification of metabolites of oridonin in rats with a single run on UPLC-Triple-TOF-MS/MS system based on multiple mass defect filter data acquisition and multiple data processing techniques, *J. Chromatogr. B: Anal. Technol. Biomed. Life Sci.*, 2015, **1006**, 80–92.

26 B. Li, H. Zhou, G. Yang, F. Han, Y. Li, Y. Gao, J. Gao, F. Zhang and L. Sun, *In vivo* study of erysolin metabolic profile by ultra high performance liquid chromatography coupleded to Fourier transform ion cyclotron resonance mass spectrometry, *J. Chromatogr. B: Anal. Technol. Biomed. Life Sci.*, 2018, **1072**, 173–181.

27 X. Zhang, J. Yin, C. Liang, Y. Sun and L. Zhang, UHPLC-Q-TOF-MS/MS Method Based on Four-Step Strategy for Metabolism Study of Fisetin *in vitro* and *in vivo*, *J. Agric. Food Chem.*, 2017, **65**, 10959–10972.

28 C. J. Liang, X. Zhang, X. P. Diao, M. Liao, Y. P. Sun and L. Zhang, Metabolism profiling of nevadensin *in vitro* and *in vivo* by UHPLC-Q-TOF-MS/MS, *J. Chromatogr. B: Anal. Technol. Biomed. Life Sci.*, 2018, **1084**, 69–79.

29 X. Y. Fan, X. C. Liu, C. F. Meng, R. N. Liu, Z. J. Zhang and C. Y. Wang, Metabolites study on 5-O-methylvisammioside *in vivo* and *in vitro* by ultra high performance liquid chromatography coupled to quadrupole time-of-flight mass spectrometry, *J. Sep. Sci.*, 2019, **42**(12), 2107–2114.

30 J. T. Yin, Y. L. Ma, C. J. Liang, J. Gao, H. Wang and L. T. Zhang, A Systematic Study of the Metabolites of Dietary Acacetin *in vivo* and *in vitro* Based on UHPLC-Q-TOF-MS/MS Analysis, *J. Agric. Food Chem.*, 2019, **67**, 5530–5543.

31 K. B. Scheidweiler, M. J. Y. Jarvis and M. A. Huestis, Nontargeted SWATH acquisition for identifying 47 synthetic cannabinoid metabolites in human urine by liquid chromatography-high-resolution tandem mass spectrometry, *Anal. Bioanal. Chem.*, 2015, **407**, 883–897.